Electronic Supplementary Information

First dual binder of miroRNA-146a and monomeric tau: A novel approach for multitargeted therapeutics for neurodegenerative diseases

Moustafa T. Gabr[a*] *and* Florent Barbault[b]

[a]*Department of Radiology, Stanford University School of Medicine, Stanford, CA, 94305. Email: gabr2003@gmail.com*
[b]*Universite de Paris, ITODYS, CNRS, UMR 7086, 15 rue J-A de Baïf, F-75013, Paris, France*

Contents

Experimental S3
Sequence of pre-miRNA146a S7
Chemical structure of MG-1102 S7
Relative fluorescence intensity at different time points upon incubation of fluorophore-labeled pre-miRNA-146a in the presence and absence of recombinant Dicer S8
A schematic illustration of the workflow adapted in this study to identify small molecules targeting both tau and miRNA-146a S8
Dose-response curves of MG-1102 in FRET assay using double-labeled pre-miRNA146a in the presence of SH-SY5Y cell lysate S9
Changes in relative fluorescence intensity in Dicer-mediated cleavage of double fluorophore-labeled pre-miRNA195 in the absence and presence of MG-1102 S9
Changes in relative fluorescence intensity in Dicer-mediated cleavage of double fluorophore-labeled pre-miRNA124 in the absence and presence of MG-1102 S10
Changes in relative fluorescence intensity in Dicer-mediated cleavage of double fluorophore-labeled pre-miRNA212 in the absence and presence of MG-1102 S10
Variation in the emission intensity (I/I_0) of ThT in the presence and absence of MG-1102 (10 μM) in response to aggregation of α-syn oligomers S11
Variation in the emission intensity (I/I_0) of ThT in the presence and absence of MG-1102 (10 μM) in response to aggregation of amyloid-beta 42 oligomers S11
Dose-response curves of MG-1102 in cellular tau FRET assay using WT tau S12
Dose-response curves of MG-1102 in cellular tau FRET assay using P301L tau S12
Plot of integrated ITC data for the exothermic interaction between MG-1102 and WT tau S13
The effect of MG-1102 (10 μM) on microtubules assembly *in vitro* promoted by wild type

tau S13
Cell viability % of rat primary cortical neurons co-incubated with tau oligomers as determined by MTT assay in absence and presence of MG-1102, curcumin, and MK-886 S14
Relative fluorescence units derived from daunorubicin that has accumulated within HCT cells expressing P-glycoprotein S14
Relative luminescence units derived from luciferase-based ATP detection that correlates with P-gp-dependent ATP consumption S15
Computational details
PAMPA-BBB permeability (P_e ×10^{-6} cm/s) of MG-1102 and controls expressed as P_e S15
In vitro pharmacokinetic profile of MG-1102 S20
S20
References S21

Experimental:

Stock solutions for fluorescence experiments

All solutions used in fluorescence experiments were filtered through 0.22 μm Millipore filters. Oligonucleotides were purchased from GenScript and purified by semiprep HPLC and characterized by electrospray ionization (ESI). Tris(hydroxymethyl)aminomethane hydrochloride(Tris–HCl) buffer (pH 7.4, RNAse-free) was used to prepare stock solutions and all working solutions used in the FRET assay.

Dicer-based assay for pre-miRNA-146a binding

The assay plates were black 384-well plates (Greiner). Solutions of tested compounds from the chemical library (10 μL) were applied to 384-well plates at a final concentration of 10 μM in a single dose screening. Subsequently, pre-miRNA-146a beacon solution (20 μL) was added to each well (final concentration 50 nM) and the plates were incubated at room temperature for 30 min. Human recombinant Dicer (0.25 U, Genlantis) was added to the reaction mixtures and the fluorescence signal was measured after 5 hours incubation. Measurements were done using an LF502 Nanoscan FLT-TRF (IOM, Berlin, Germany), equipped with a laser as excitation source (λ_{ex} = 485 nm, λ_{em} = 535 nm). The dose-response curves were analyzed by nonlinear regression using GraphPad Prism 8.0.2 (GraphPad Software, Inc., La Jolla, CA, USA). Each data point from this assay represents the average of three independent measurements. Error bars represent standard deviation. Determination of K_D value was assessed using the same procedure by replacing molecular beacon with fluorophore-labeled oligonucleotide.

Validation of the Dicer-based assay for high-throughput screening (HTS):

Z' factor was calculated using the following equation:[1]

$$Z' \text{ factor} = 1 - \frac{(S.D. + ve) + (S.D. - ve)}{(mean + ve) - (mean - ve)}$$

Where, S.D. +ve : Standard deviation of the positive control.

S.D. –ve: Standard deviation of the negative control.

Mean +ve : mean of the positive controls

Mean –ve : mean of the negative controls

Quantitative RT-PCR

TRIzol reagent (Invitrogen) was used to extract total RNA according to the provider's protocol. NanoDrop spectrophotometer was used to quantify RNA concentrations extracted. MicroRNA analysis using TaqMan assay was performed using TaqMan microRNA assay (ThermoFisher) according to the manufacturer's protocol to quantify the expression of mature miRNAs. Relative expressions were calculated by using the comparative threshold cycle (Ct) method.

Reporter luciferase assays

The assay was performed as reported previously.[2] The firefly luciferase activity was measured after 4 days of treatment on cell lysates by using the Luciferase assay (Promega). The luciferase activities were normalized by the amount of total cell protein, determined on the cell lysate by using the Bradford assay (Biorad).

Cellular tau fluorescence-based assay

The selected compounds were screened in a single-dose format (10 μM) adopting the procedure previously described for the screen as well as transfection of cells with tau-GFP/RFP.[3] Expression of tau-GFP/RFP in SH-SY5Y cells was confirmed using fluorescence microscopy. Compounds were dispensed as DMSO stock solutions (50 nL) to the 384-well plates (PN 781209, Greiner Bio-One) at a final concentration of 10 μM. Cells (1 millions cell/mL concentration) were dispensed to the assay plates (50 μL/well) and the plates were incubated for 2 hours at room temperature. Measurements were done using an LF502 Nanoscan FLT-TRF (IOM, Berlin, Germany). Hit compounds were identified by the ability to attenuate FRET signal five times the standard deviation relative to the mean. Fluorescent compounds were removed from further evaluation for potential interference as false positives. We next evaluated the dose-response profile of MG-1102 and determined the respective IC_{50} value. The dose-response curve was analyzed by nonlinear regression using GraphPad Prism 8.0.2 (GraphPad Software, Inc., La Jolla, CA, USA). Each data point from this assay represents the average of three independent measurements. Error bars represent standard deviation.

SPR screening

BIAcore S200 was used for SPR screening of the affinity of MG-1102 to WT tau. Immobilization of WT tau (20 μg/ml) on CM5 sensor chip (Biacore, GE Healthcare) was done by amine coupling using 0.4 M 1-ethyl-3-(3-dimethylaminopropyl)carbodiimide hydrochloride and 0.1 M N-hydroxysuccinimide.

Stock solution of MG-1102 was prepared in DMSO at 1 mM final concentration. Samples were then serially diluted while maintaining final DMSO concentration to 5% in all tested concentrations. Tested dilutions in HEPES (pH 7.5) containing 5% DMSO and 0.05% Tween20 were allowed to flow through both ligand-captured flow cells and reference flow cells at the same rate (30 μl/min) and contact time (120 sec). Solvent correction was included to avoid the impact of DMSO on surface plasmon effect during binding analysis. Extra wash of the flow system using 50% DMSO in HEPES buffer was then performed following each run. Kinetic analysis was performed at 25 °C. Equilibrium dissociation rate constant (K_d) values was calculated using Biacore S200 Evaluation software.

Isothermal titration calorimetry (ITC)

Stock solutions of WT tau and MG-1102 were dialyzed against HEPES buffer (pH 7.5) containing 100 mM NaCl. A final DMSO concentration of 2% v/v was added to both stock solutions. ITC experiments were performed using GE MicroCal iTC 200 isothermal titration calorimeter. Titration experiments were conducted by injecting MG-1102 (0.5 mM) over a sample cell containing WT tau (50 μM). The resultant heats per injection were subtracted from the data for the MG-1102/WT tau interaction. The data was fitted using non-linear least squares regression to obtain the enthalpy change (Δ H) and equilibrium binding constants (K_B) of the bimolecular interaction. Data were processed using MicroCal Origin software.

Microscale Thermophoresis (MST)

MST study was performed as previously described for investigating the interaction of small molecules with WT tau.[4]

Cell viability assay in SH-SY5Y cells

SH-SY5Y cells expressing miRNA-146a were grown in Roswell Park Memorial Institute medium (RPMI) supplemented with 2 mM L-glutamine, 100 UI/mL penicillin, 100 μg/mL streptomycin and 10% (v/v) fetal

bovine serum (FBS). Cells were maintained in culture dishes at 37 °C in a saturated humidity atmosphere containing 95% air and 5% CO_2. SH-SY5Y cells were plated at a density of 5 x 10^6 cells/plate in 100 mm plates (Corning) and transfected with WT tau for 24 hours as previously reported.[3] Transfected cells were plated (5000 cells/well) in 96-well plates (Corning). Tested compounds at various concentrations were added to the assay plates as well as negative controls (DMSO). The assay plates were incubated for 72 hours. Cell viability was determined by measuring mitochondrial activity using the MTT (3-(4,5-dimethylthiazole-2-yl)-2,5-diphenyltetrazolium bromide) assay. After the incubation time, the medium was removed and cells were incubated with 100 µl MTT (0.5 mg/ml) for 1 h. After that, the solution was removed, the formazan formed solubilized in100 µl of 0.1N HCl in 90 % (v/v) 2-propanol and the absorbance was measured at 570 nm using a microplate reader (BioRad 680, USA).

***In vitro* blood-brain barrier permeability**

The ability of MG-1102 to penetrate blood−brain barrier (BBB) was evaluated using a parallel artificial membrane permeation assay (PAMPA) for BBB according to the method established by Di et al.[5] Donepezil and caffeine were used as reference compounds in the PAMA assay. The donor microplate (96-wellfilter plate, PVDF membrane) and the acceptor microplate (indented 96-well plate) were both obtained from Millipore. The acceptor 96-well microplate was filled with 300 µL of PBS/EtOH (7:3), and the filter membrane was impregnated with 10 mL of porcine brain lipid (PBL) in dodecane (20 mg/mL). The compound was dissolved in DMSO at a concentration of 5 mg/mL followed diluting 50-fold with a mixture of PBS/EtOH (7:3) to give a final concentration of 100 µg/mL. After that, 200 µL of diluted solution and 300 µL of PBS/EtOH (7:3) were added to the donor wells. The donor filter plate was placed on the acceptor plate to make the underside of filter membrane in contact with buffer solution. After leaving this sandwich assembly for 16 h at 25 °C, the donor plate was removed, and the concentrations of tested compound in the acceptor, donor and reference wells were measured with a UV plate reader. Each sample was analyzed three independent runs in four wells.

Pharmacokinetic profiling

The assays for determining pharmacokinetic profile were performed as previously described.[6] The data for compound MG-1102 and positive controls are listed in Table S2.

***In vitro* microtubules assembly assay**

The assay was performed as previously described.[7]

Cell viability assay in primary cortical neurons

Rat (E18) primary cortical neurons were purchased from BrainBits, LLC. Cells were grown in serum free Neurobasal medium with B-27 supplement (Life Technologies), 25 µM L-glutamate, 100 U/mL penicillin, 100 µg/mL streptomycin, and 0.5 mM L-glutamine. Cells were plated in 96-well (2×10^4 cells/well) and 10 µM of tau oligomers prepared as previously described[8] were added to the plated cells. MTT assay to measure cell viability was performed as described above.

P-glycoprotein binding assay

A cellular assay kit provided by INDIGO Biosciences (Product # HPGP-48) was used. The assay was performed following the manufacturer's protocol.

P-glycoprotein ATPase assay

The assay was performed using Promega kit (Catalog # V3591) by following the supplier's protocol.

```
   c     -----u      u     uu            c  u     g  uc
5'  cgaug       guaucc cagcu  gagaacugaauu ca ggguu ug  a
    |||||       |||||| |||||  |||||||||||| || ||||| ||  g
3'  gcuac       uauagg gucga  uucuugacuuaa gu uccag ac  u
   u     ugucuc       -     -c            a  c     -  ug
```

Figure S1. Sequence of pre-miRNA146a.

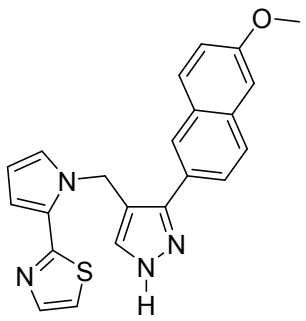

Figure S2. Chemical structure of MG-1102.

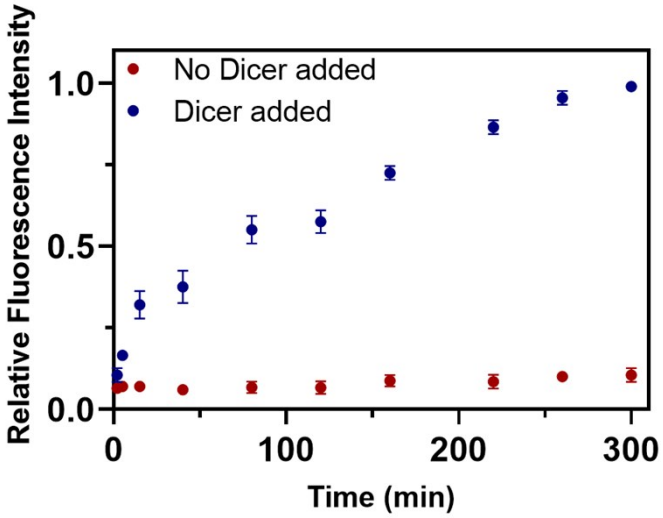

Figure S3. Relative fluorescence intensity at different time points upon incubation of 50 nM fluorophore-labeled pre-miRNA-146a in the presence and absence of 0.25 U recombinant Dicer. Error bars represent standard deviation (n= 3).

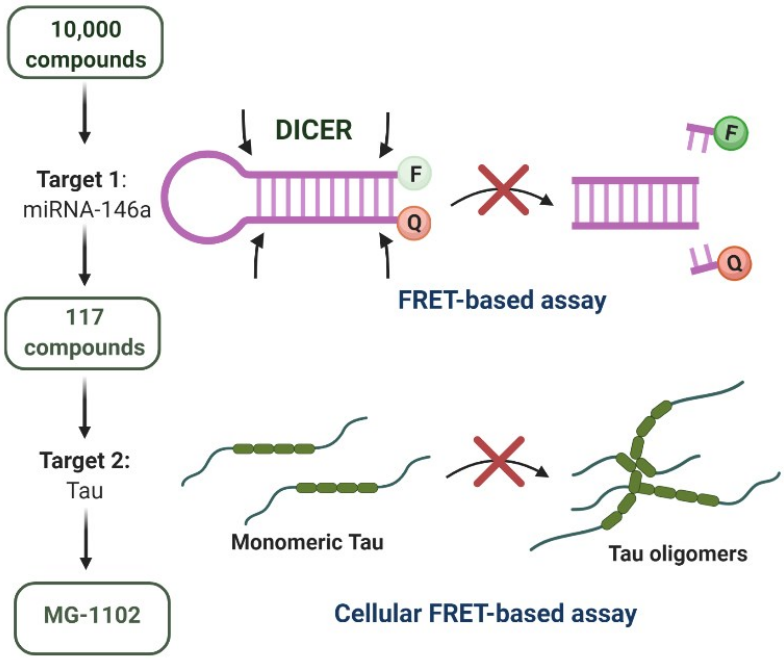

Figure S4. A schematic illustration of the workflow adapted in this study to identify small molecules targeting both tau and miRNA-146a.

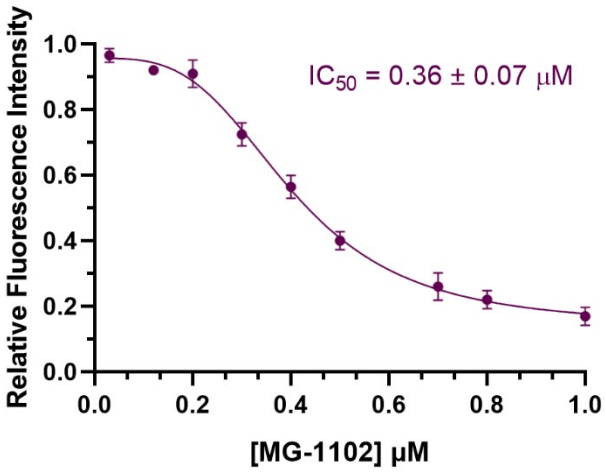

Figure S5. Dose-response curves of MG-1102 in FRET assay using double-labeled pre-miRNA146a in the presence of SH-SY5Y cell lysate. Error bars represent standard deviation (n = 3).

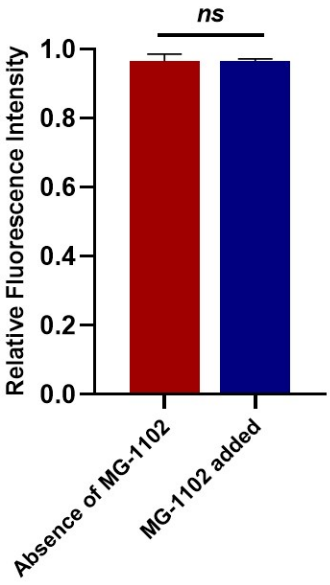

Figure S6. Changes in relative fluorescence intensity in Dicer-mediated cleavage of double fluorophore-labeled pre-miRNA195 in the absence and presence of MG-1102 (10 μM). Error bars represent standard deviation (n = 3). ns denotes non-significant difference.

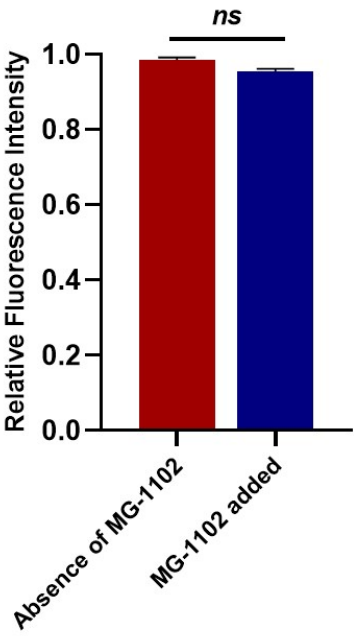

Figure S7. Changes in relative fluorescence intensity in Dicer-mediated cleavage of double fluorophore-labeled pre-miRNA124 in the absence and presence of MG-1102 (10 μM). Error bars represent standard deviation (n = 3). ns denotes non-significant difference.

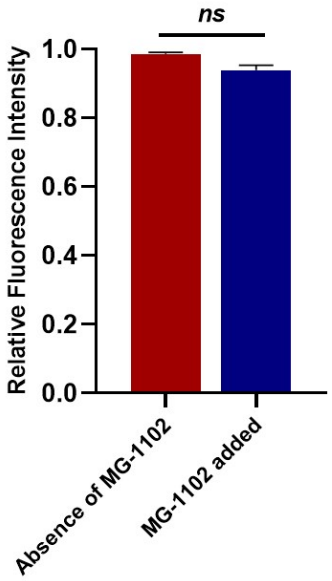

Figure S8. Changes in relative fluorescence intensity in Dicer-mediated cleavage of double fluorophore-labeled pre-miRNA212 in the absence and presence of MG-1102 (10 μM). Error bars represent standard deviation (n = 3). ns denotes non-significant difference.

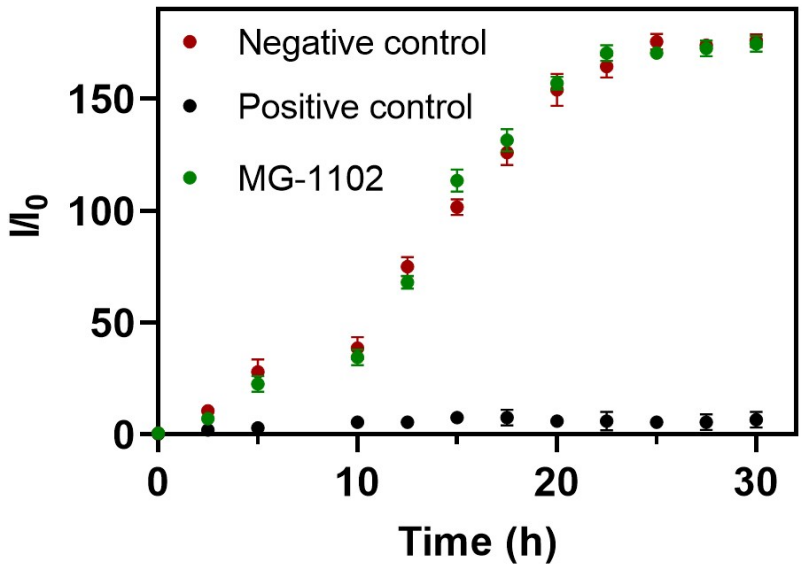

Figure S9. Variation in the emission intensity (I/I_0) of ThT in the presence and absence of MG-1102 (10 μM) in response to aggregation of α-syn oligomers (100 μM), λ_{ex} = 440 nm, [ThT] = 5 mM. Negative control denotes to the absence of MG-1102. Positive control denotes to Epigallocatechin gallate. Error bars represent standard deviation (n = 3).

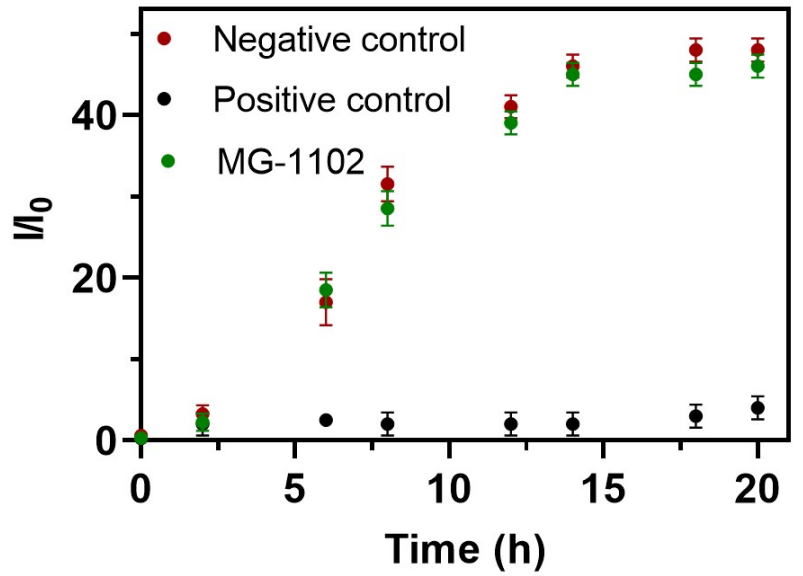

Figure S10. Variation in the emission intensity (I/I_0) of ThT in the presence and absence of MG-1102 (10 μM) in response to aggregation of amyloid-beta 42 oligomers (100 μM), λ_{ex} = 440 nm, [ThT] = 5 mM. Negative control denotes to the absence of MG-1102. Positive control denotes to tannic acid. Error bars represent standard deviation (n = 3).

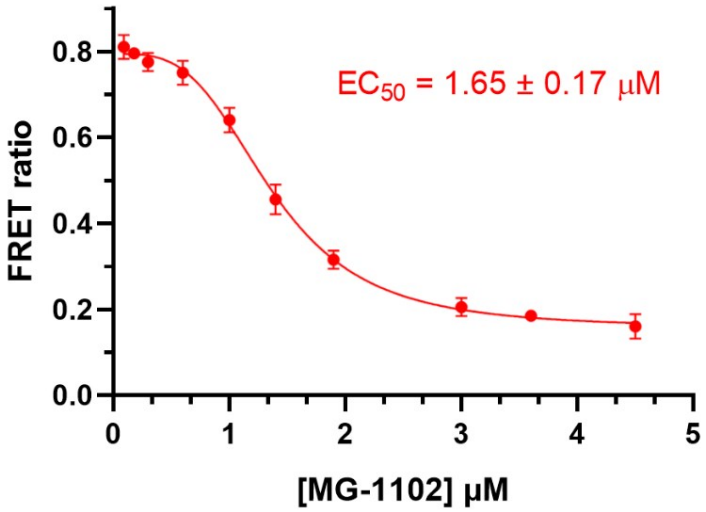

Figure S11. Dose-response curves of MG-1102 in cellular tau FRET assay using WT tau. Error bars represent standard deviation (n = 3).

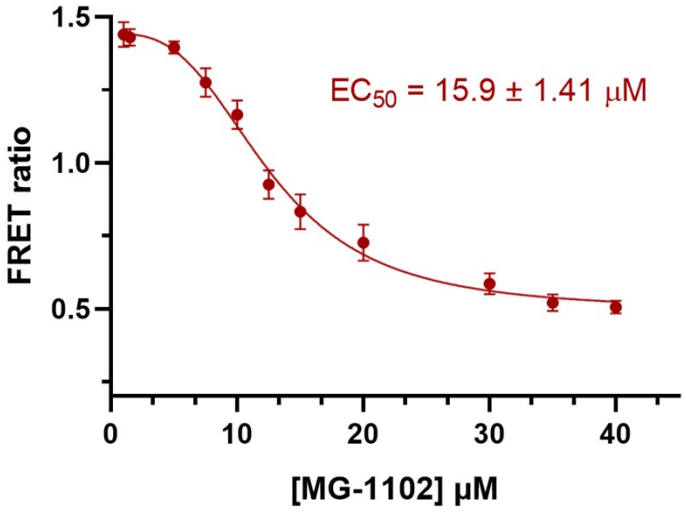

Figure S12. Dose-response curves of MG-1102 in cellular tau FRET assay using P301L tau. Error bars represent standard deviation (n = 3).

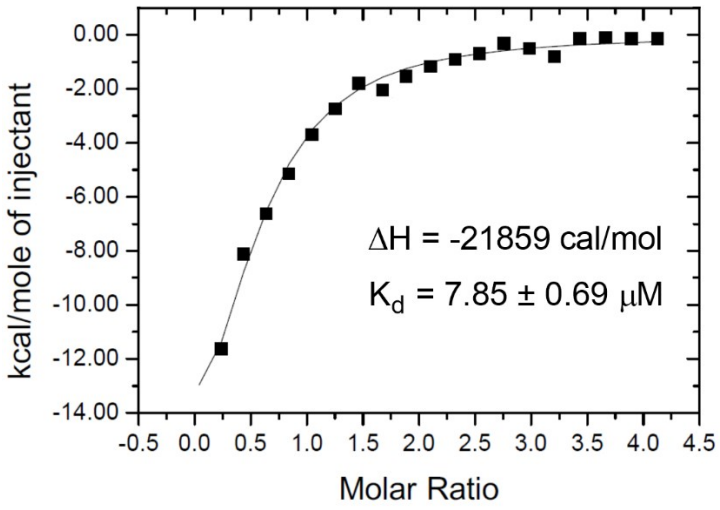

Figure S13. Plot of integrated ITC data for the exothermic interaction between MG-1102 and WT tau (50 μM). The solid line represents the best least-squares fit to the data.

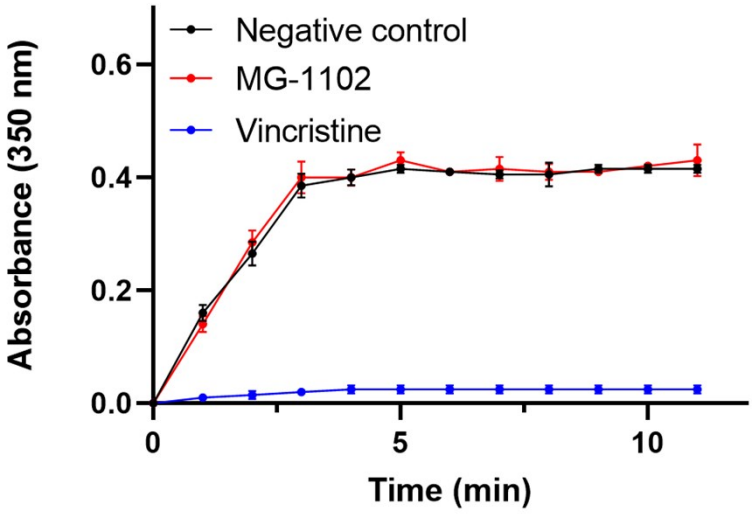

Figure S14. The effect of MG-1102 (10 μM) on microtubules assembly *in vitro* promoted by wild type tau. Vincristine (10 μM) is used as a positive control. Solvent was used as negative control. Error bars represent standard deviation (n = 3).

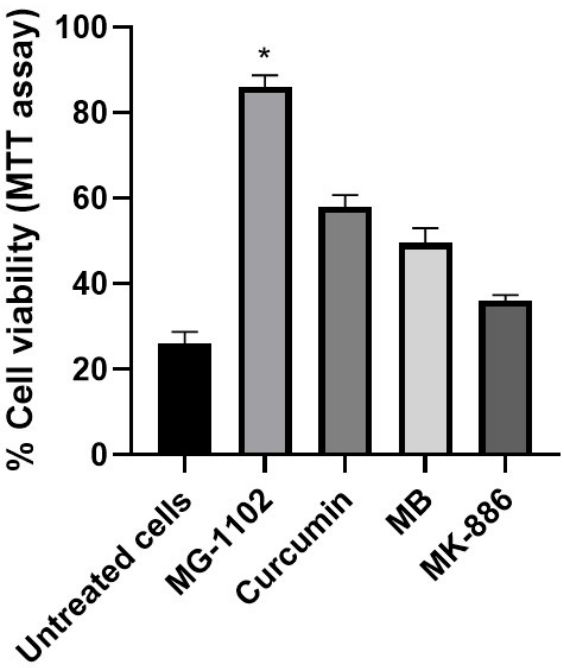

Figure S15. Cell viability % of rat primary cortical neurons co-incubated with tau oligomers (10 μM) as determined by MTT assay in absence and presence of 10 μM of MG-1102, curcumin, methylene blue (MB), and MK-886. Error bars represent standard deviation (n = 3, * $p < 0.05$ relative to untreated cells).

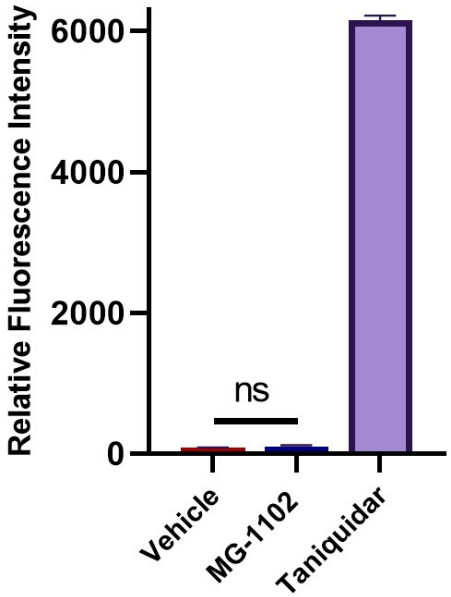

Figure S16. Relative fluorescence units derived from daunorubicin that has accumulated within HCT cells expressing P-glycoprotein. There is an inverse-relationship between the rate of probe efflux and measured intracellular fluorescence. Competition has been done with 10 μM of MG-1102 and Tariquidar (a potent reference inhibitor of P-glycoprotein). Error bars represent standard deviation (n = 3). ns denotes non-significant difference.

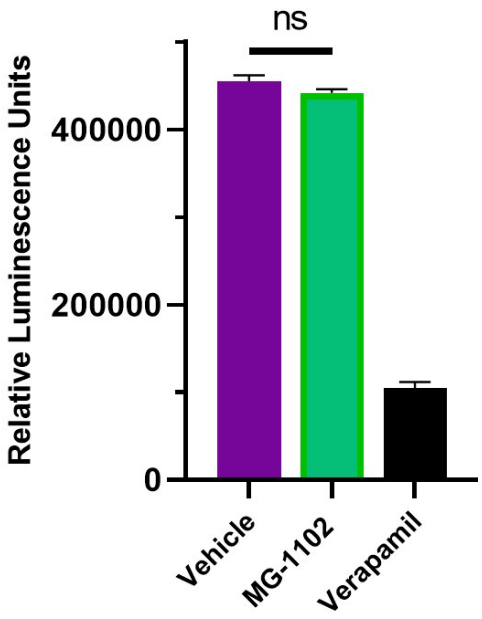

Figure S17. Relative luminescence units derived from luciferase-based ATP detection that correlates with P-gp-dependent ATP consumption. The assay was done in the absence and the presence of MG-1102 (10 mM) using verapamil as a positive control. Error bars represent standard deviation (n = 3). ns denotes non-significant difference.

Computational details:

The structure of pre-miRNA-146a was constructed from its sequence with three different web servers dedicated to this task: 3dRNAweb,[9] RNAcomposer[10,11] and MC-Fold MC-Sym.[12] Each predicted structure was then immersed in a rectangular box of TIP3P water molecules extending to a distance of 10 Å from any RNA atoms and subjected to a molecular dynamic (MD) simulation. To do this task the Amber16 software package[13] was employed with the RNA.OL3 force-field specifically design for RNA.[14,15] All conducted MD pursue a similar protocol: first the whole system is minimized with 5000 steps of steepest descent followed by 25000 steps of conjugated-gradient. Then the system is heated to 300 K in two stages, a first 50 ps in the NVT ensemble for 0 to 50 K and then 100 ps for 50 to 300 K in the NTP ensemble. During these steps, all solute atoms were weakly restrained with a harmonic potential of 0.5 $kcal.mol^{-1}.Å^{-1}$. Finally, restraints were removed and production trajectories of 50 ns were obtained in the NTP ensemble at 300 K. To check the equilibration, root mean square deviation (RMSD) were computed for all MDs simulations. The cpptraj post-processing software[16] was used for clustering the trajectories with a density-based technique[17] and determinate RNA representative structures. Other technical details may be found in previously published studies.[18]

MG-1102 (Figure S2) was built with the maestro software[19] and molecular docking calculations were performed with the Autodock 4.2 software[20] specifically modified, with the help of an artificial intelligence procedure, to cope with the RNA as target.[21] This software modification has already been validated and proven its reliability.[22,23] The Lamarckian Genetic Algorithm[24] was employed for the global optimum binding position search. For each molecular docking investigation, extensive docking computations with 100 independent computations with 100 poses, leading thus to 10 000 poses, was

realized to get a position as accurate as possible. The resulting docking structures were then clustered according to a RMSD lower than 2 Å. The conformation selected was the one which presented the lowest docking free energy of binding in the most populated cluster.[25]

Results and discussion:

Computational studies were addressed to elucidate the structural interaction between MG-1102 and pre-miRNA-146a. To date, there is no experimental structure available for pre-miRNA-146a. However, several tools exist which aim to predict a 3D RNA structure from its 1D sequence. In this work three of these webtools were employed, RNA composer, MC-Fold /MC-Sym and 3dRNAweb. All of these techniques provided the same 2D folding, presented in Figure S18 but also subtle 3D structural differences as shown on the top of Figure S19. Starting from these predicted miRNA-146a structures, three molecular dynamics simulations were conducted for 50 ns in water boxes.

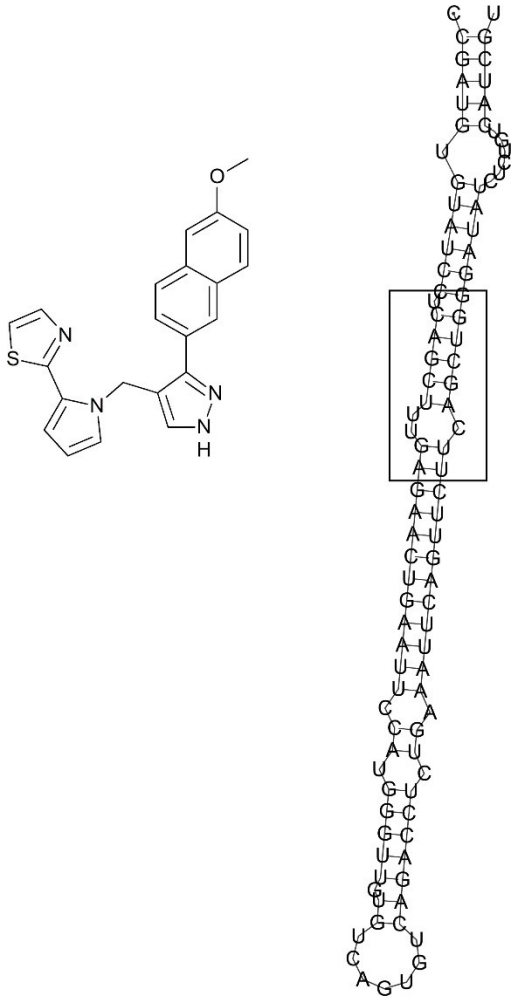

Figure S18. Left: Chemical structure of MG-1102 compound. Right: 2D folding of pre-miRNA146a. The interacting site is highlighted with a square.

As expected, the three independent molecular dynamics simulations shown a relative flexibility of the bulges and internal loops of the pre-miRNA-146a structures whereas the helices parts remain stables. To identify a representative structure of the RNA which could then been employed in the molecular

docking step, all trajectories were gathered and a subjected to a density-based clustering. Interestingly the most probable cluster is observed for all trajectories, indicating that, whatever is the started pre-miRNA-146a, the structure presented in the bottom of Figure S19 is always encountered. Therefore, this consensus structure was then employed as target for the molecular docking steps.

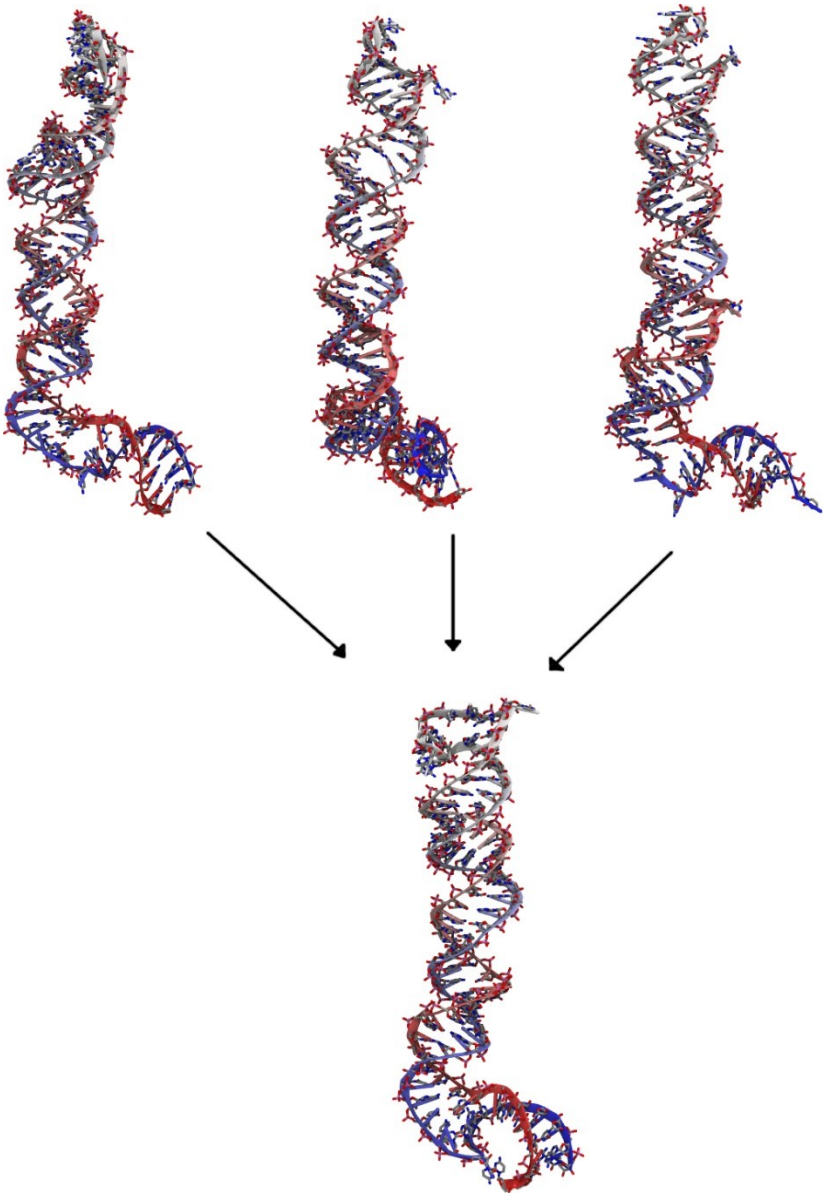

Figure S19. Top: visualization of the three predicted structural model of pre-miRNA-146a obtained with, from left to right, RNA composer, MC-Fold MC-Sym and 3dRNAweb. Bottom: the consensus structure of pre-miRNA-146a identified by clustering the three 50 ns of molecular dynamics simulations of the above models.

A two-step procedure was conducted for molecular docking computations. First, an extensive molecular docking was made on the whole pre-miRNA-146a structure to identify the RNA interacting site. The 100 best docking poses were analysed and are presented on the left part of Figure S20. This area, presented with a square on figure S18 and a circle in figure S20, is delineated from residues U14 to A23 and U74 to G81 and contains, as specific structural elements, the mismatch U14 and the internal loop

U19-G22/U73-A75. On this area, one unanticipated finding was the observation of two mode of interactions for MG-1102. To gain insights on the mode of interaction a supplemental similar molecular docking investigation was made located on the delineated area. For this new docking investigation, the analyses of the 100 best docking poses highlighted two mode of interaction. The first one, located on the major groove of this area are observed in 66% of the poses and present an average docking energy of -8.24 kcal/mol. These structures display at least one hydrogen-bond with either one phosphate group or a nucleic base. The second one, observed in 34% of the docking poses, has an average docking energy of -7.12 kcal/mol and is located on the minor groove of pre-miRNA-146a interacting solely through Van der Waals interaction. The fact that a compound interacts only with dispersive forces such as Van der Waals is usually the sign of a false positive poses in molecular docking computations.[26] Therefore, it was decided to launch two 50 ns of molecular dynamics simulations for pre-miRNA-146a/MG-1102 complex for both ligand positions.

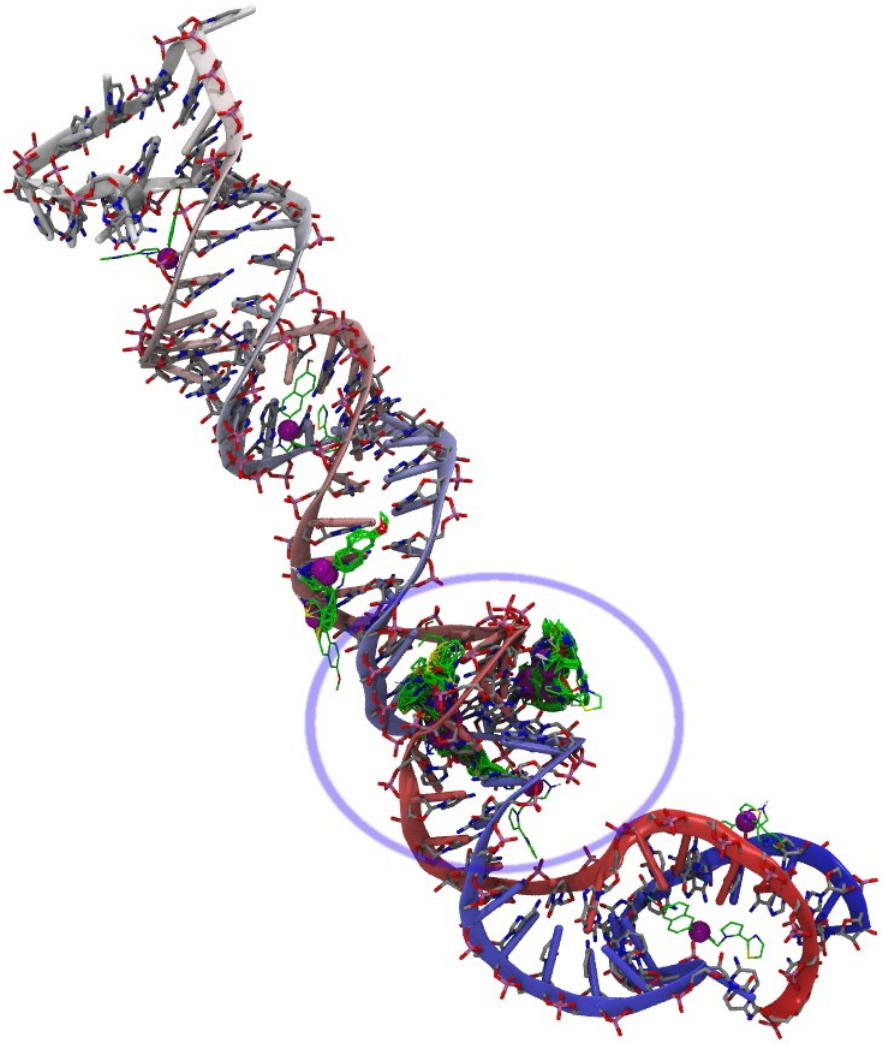

Figure S20. The 100 best docking positions of MG-1102 onto the pre-miRNA-146a whole structure. On this figure, the carbon atoms of RNA and ligand are, respectively shown with silver and green colours. The centre of gravity of MG-1102 is displayed with a purple sphere. The interacting area is delineated with a blue circle.

Visualizations of the molecular dynamics trajectories lead us to a definite answer for the mode of interaction of MG-1102. Indeed, when MG-1102 is located in the minor groove with solely Van der Waals interactions, the ligand quickly moves onto the RNA surface during the first 10 ns indicating that there's no specific interaction. Around 12.6 ns MG-1102 dissociates from its RNA target and goes solvated. On the other hand, when MG-1102 is inserted in the major groove of pre-miRNA-146a this one remains inside its target and several molecular interactions occurred. Figure S20 illustrates the main interaction of MG-1102 with pre-miRNA-146a.

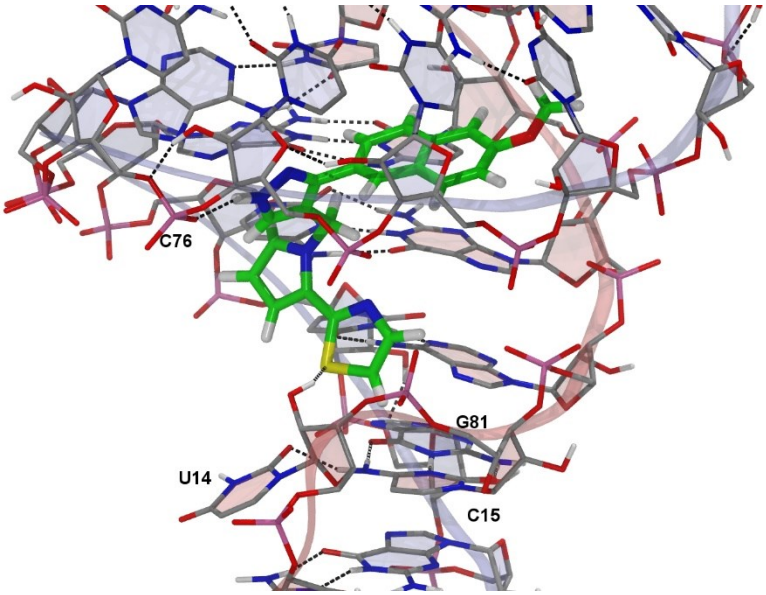

Figure S21. MG-1102 structural interaction with pre-miRNA-146a. The RNA and ligand carbons are presented with, respectively, silver and green colours whereas other atoms are referred with CPK colours. hydrogen-bonds are displayed with dashed lines.

As shown on Figure S21, MG-1102 makes two hydrogen bonds with pre-miRNA-146a. The first one concern the sulphur atoms of the ligand and targets the 3' hydroxyl group of U14 which makes a triple base with C15 and G81. The other hydrogen bond involves the NH atoms of the pirazolo ring of MG-1102 and targets one oxygen of the C76 phosphodiester group. Finally, the diphenyl moiety is inserted in the pocket made by the U19-G22/U73-A75 internal loop displaying hydrophobic interaction.

Table S1. PAMPA-BBB permeability (P_e ×10^{-6} cm/s) of MG-1102 and controls expressed as P_e and their predictive penetration to the CNS.

Comp.	P_e (×10^{-6} cm/s)	Predication of CNS penetration
MG-1102	27.1	High
Donepezil	23.2	High
Caffeine	2.15	Low

Table S2. *In vitro* pharmacokinetic profile of MG-1102.

Test	MG-1102	Control compound
Stability in simulated fluids ($t_{1/2}$, min)		
Gastric (pH 1.6)	455	>500[a]
Intestinal (pH 6.5)	>500	490[b]
Stability in human plasma (% remaining at 120 min)	98	2.99[c]
CACO cell permeability		
P_{app}, A ⟶ B (10^{-6} cm/s)	17.5	34.7[d]
P_{app}, B ⟶ A (10^{-6} cm/s)	32.1	38.1[d]
Stability in rat liver microsomes ($t_{1/2}$, min)	>200	5.4[e]
Cytotoxicity in HEL 299 cells (IC_{50}, µM)	>50	25.9[f]

[a]Cyclosporine was used as a control; [b]Erythromycin was used as a control; [c]Propantheline was used as a control; [d]Propranolol was used as a control; [e]Verapamil was used as a control; [f]Mitoxantrone was used as a control.

References:

1 J. H. Zhang, T. D. Chung and K. R. Oldenburg, *J. Biomol. Screen.*, 1999, **4**, 67-73.
2 C. Staedel, T. P. A. Tran, J. Giraud, F. Darfeuille, A. Di Giorgio, N. J. Tourasse, F. Salin, P. Uriac and M. Duca, *Sci. Rep.*, 2018, **8**, 1667.
3 C. H. Lo, C. K. Lim, Z. Ding, S. P. Wickramasinghe, A. R. Braun, K. H. Ashe, E. Rhoades, D. D. Thomas and J. N. Sachs, *Alzheimers Dement.*, 2019, **15**, 1489-1502.
4 R. Kiss, G. Csizmadia, K. Solti, A. Keresztes, M. Zhu, M. Pickhardt, E. Mandelkow and G. Tóth, *ACS Chem. Neurosci.*, 2018, **9**, 2997-3006.
5 L. Di and E. H. Kerns, *Curr. Opin. Chem. Biol.*, 2003, **7**, 402-408.
6 (a) D. K. Tosh, A. Finley, S. Paoletta, S. M. Moss, Z.-G. Gao, E. T. Gizewski, J. A. Auchampach, D. Salvemini and K. A. Jacobson, *J. Med. Chem.*, 2014, **57**, 9901-9914. (b) 1. D. K. Tosh, J. Padia, D. Salvemini and K. A. Jacobson, *Purinergic Signal.*, 2015, **11**, 371-387.
7 C. Feijoo, D. G. Campbell, R. Jakes, M. Goedert and A. Cuenda, *J. Cell Sci.*, 2005, **118**, 397-408.
8 C. A. Lasagna-Reeves, D. L. Castillo-Carranza, M. J. Guerrero-Muoz, G. R. Jackson and R. Kayed, *Biochemistry*, 2010, **49**, 10039-10041.
9 J. Wang, J. Wang, Y. Huang and Y. Xiao, *Int. J. Mol. Sci.*, 2019, **20**, 4116.
10 M. Popenda, M. Szachniuk, M. Antczak, K. J. Purzycka, P. Lukasiak, N. Bartol, J. Blazewicz and R. W. Adamiak, *Nucleic Acids Res.*, 2012, **40**, e112-e112.
11 M. Antczak, M. Popenda, T. Zok, J. Sarzynska, T. Ratajczak, K. Tomczyk, R. W. Adamiak and M. Szachniuk, *Acta Biochim. Pol.*, 2016, **63**, 737-744.
12 M. Parisien and F. Major, *Nature*, 2008, **452**, 51-55.
13 D. A. Case, R. M. Betz, D. S. Cerutti, T. E. Cheatham, T. A. Darden, R. E. Duke, et al. AMBER 2016. University of California, San Francisco; 2016.
14 A. Perez, I. Marchan, D. Svozil, J. Sponer, T. E. Cheatham, 3rd, C. A. Laughton and M. Orozco, *Biophys. J.*, 2007, **92**, 3817-3829.
15 M. Zgarbová, M. Otyepka, J. Šponer, A. Mládek, P. Banáš, T. E. Cheatham and P. Jurečka, J. Chem. Theory Comput., 2011, **7**, 2886-2902.
16 D. R. Roe and T. E. Cheatham, 3rd, *J. Chem. Theory Comput.*, 2013, **9**, 3084-3095.
17 M. Ester, H.-P. Kriegel, X. Xu, A Density-Based Algorithm for Discovering Clusters in Large Spatial Databases with Noise. Proceedings of the Second International Conference on Knowledge Discovery and Data Mining, AAAI Press. 1996, 226-231.
18 L. Aixiao, B. Florent, M. François, D. Michel and W. Baoshan, *J. Mol. Struc.-THEOCHEM*, 2008, **849**, 62-75.
19 Schrödinger Release 2020-1: Maestro [Internet]. New York, NY: Schrödinger, LLC; Disponible sur: https://www.schrodinger.com/
20 G. M. Morris, R. Huey, W. Lindstrom, M. F. Sanner, R. K. Belew, D. S. Goodsell and A. J. Olson, *J. Comput. Chem.*, 2009, **30**, 2785-2791.
21 F. Barbault, L. Zhang, L. Zhang and B. T. Fan, *Chemometer. Intell. Lab*, 2006, **82**, 269-275.
22 F. Barbault, B. Ren, J. Rebehmed, C. Teixeira, Y. Luo, O. Smila-Castro, F. Maurel, B. Fan, L. Zhang and L. Zhang, *Eur. J. Med. Chem.*, 2008, **43**, 1648-1656.
23 M. Duca, V. Malnuit, F. Barbault and R. Benhida, *Chem. Commun. (Camb)*, 2010, **46**, 6162-6164.
24 G. M. Morris, D. S. Goodsell, R. S. Halliday, R. Huey, W. E. Hart, R. K. Belew and A. J. Olson, *J. Comp. Chem.*, 1998, **19**, 1639-1662.
25 C. Teixeira, N. Serradji, F. Maurel and F. Barbault, *Eur. J. Med. Chem.*, 2009, **44**, 3524-3532.
26 F. Barbault and F. Maurel, *Expert Opin. Drug Discov.*, 2015, **10**, 1047-1057.